RSC Advances

ROYAL SOCIETY OF CHEMISTRY

www.rsc.org/advances

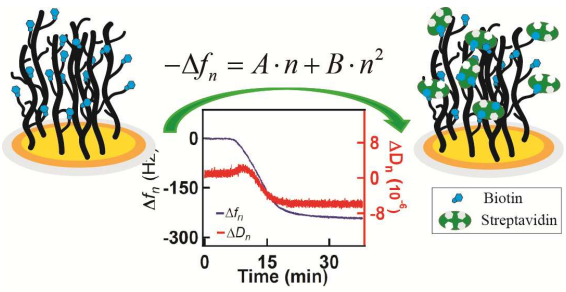

Quartz crystal microbalance was successfully applied to quantitatively analyze biomolecular interactions using a poly(ethylene glycol) matrix and equations for impedance analysis of frequency changes at multiple overtones.

RSC Advances

ARTICLE

Quartz Crystal Microbalance as a tool for biomolecular interaction study

Received 00th January 20xx,
Accepted 00th January 20xx

DOI: 10.1039/x0xx00000x

www.rsc.org/

Yuanzi Wu[a], Hongwei Ma[a], Dayong Gu[b] and Jian'an He[b]*

Abstract: Quartz crystal microbalance (QCM) and surface plasma resonance (SPR) are two typical solid-phase based technologies for biomolecular interaction studies. Although QCM is more affordable than SPR, the popularization of QCM as a biosensor is limited by the nonideal behavior that complicates the quantitative interpretation of frequency changes, especially the viscoelastic factor, implying that caution should be taken in interpreting QCM responses for large molecular applications. A poly(ethylene glycol) based matrix (PEG matrix) was tested on both QCM and SPR using model bait-prey pairs. Based on the dissipation monitoring technique, this matrix was found to have minimal viscoelasticity change before and after biomolecular binding. Furthermore, impedance analysis of frequency responses at multiple overtones was able to remove the viscoelastic contribution based on experimental results. Therefore, it is proved that the PEG matrix combining with the equations for impedance analysis of frequency changes at multiple overtones will facilitate the popularization of QCM as a biosensor.

Introduction

Quartz crystal microbalance (QCM) and surface plasma resonance (SPR) are two typical solid-phase based technologies for biomolecular interaction studies. As an optical biosensor, SPR measures the dry (nonhydrated) mass change due to the binding of biomolecules to the sensor surface.[1] As an acoustic biosensor, QCM measures the wet mass change.[2-4] Results of these two methods were often compared by using a defined conversion factor which relates wet mass changes from QCM to dry mass changes detected by SPR [2, 5] or by other established methods, such as radio-labeling, [6] ellipsometry and optical waveguide lightmode spectroscopy [7]. Although QCM is more affordable than SPR, the popularization of QCM as a biosensor is limited by the nonideal behavior that complicates the quantitative interpretation of frequency changes, especially the viscoelastic factor.[8-10] For example, the converting factors found in the literature were not in agreement: while there were a few cases of reported converting factors being 1 or less,[11] most researchers reported converting factors at values within the range of 1.5 ~ 10.[2, 8, 12, 13] Besides the differences of subjects under study (proteins different in size, for example), this discrepancy also caused by the different matrices of QCM sensors.

A good functional matrix will greatly enhance the performance of a biosensor in that it can: (i) increase the immobilization capacity of bait molecules; (ii) better preserve the biological activity of bait molecules; (iii) lower the background by reducing nonspecific protein adsorption; (iv) especially for QCM, minimize the nonideal behavior. For example, Fawcett et al. proposed that a thin and rigid matrix could be applied to increase the immobilization capacity while causing only small viscoelastic changes upon bait-prey recognition. [14] Although self-assembled monolayer (SAM) serves well for this purpose,[15] previous studies have indicated that a three dimensional (3D) matrix could provide a 10-fold increase of immobilized bait molecules.[16] There are a few reports on the preparation of 3D matrices for QCM as a biosensor, yet no quantitative studies were found on how the viscoelasticity change of the 3D matrices affected the frequency change. [17]

An impedance analyzer and the impulse excitation method (i.e., dissipation analysis) have been integrated into regular QCM to separate the contribution of viscoelasticity as well as other irrelevant factors.[5, 18] Recently, we have applied the impedance method to analyse the dissipation data using equations (1) to (3):

$$-\Delta f_n = A \cdot n + B \cdot n^2 \quad (1)$$

$$A = \frac{2 f_0^2 \rho_f d_f}{Z_q} \quad (2)$$

$$B = \frac{-4\pi f_0^3 \rho_{liq} \eta_{liq} d_f J_f^*}{Z_q} \quad (3)$$

where Δf_n and f_n are the frequency shift and the resonance frequency at overtone number n, respectively; $f_n = n f_0$, n = 1, 3, 5, 7, 9, 11, 13…; ρ_f and d_f are the wet film density and thickness of the deposited film in liquid, respectively; Z_q = 8.8 × 10^6 kg m^{-2} s^{-1} is the acoustic impedance of the crystalline quartz.

[a] Suzhou Institute of Nano-Tech and Nano-Bionics, Chinese Academy of Sciences, Suzhou 215125, P. R. China.
[b] Institute of Disease Control and Prevention, Shenzhen International Travel Health Care Center, Shenzhen Entry-exit Inspection and Quarantine Bureau, Shenzhen, 518033, P. R. China. E-mail: hejianan6398@163.com; Fax: +86-0755-83394162; Tel: +86-0755-83391433.

Electronic Supplementary Information (ESI) available. See DOI: 10.1039/b000000x/

The fitted value A includes only the wet mass (dry materials with entrapped liquid) contribution, free of that from viscoelastic. Respectively, the fitted value B represents the visocelasticity induced frequency change. We proposed in our previous publication [19] that this analytical method was especially suitable for biological samples because it only required one sample to be measured at multiple overtones at one time. For QCM used as a biosensor, a positive A value indicates wet mass increase upon the bait-prey recognition. A positive B value indicates rigidity increase of the system (matrix + bait-prey pair), which is equivalent to wet mass ($-\Delta f_n$) increase or dissipation factor decrease. Herein, we report the application of a poly(ethylene glycol) based matrix (PEG matrix) on both QCM and SPR, using model bait-prey pairs. Through the dissipation monitoring technique, this matrix was found to have minimal viscoelasticity change before and after bait-prey recognition. Furthermore, impedance analysis (equations (1) ~ (2)) of frequency responses at multiple overtones was able to remove the viscoelastic contribution.

Experimental

Materials and reagents

The initiator thiol (ω-mercaptoundecyl bromoisobutyrate), 11-(mercaptoundecyl)tri(ethylene glycol)(EG3-thiol), SPR, and QCM chips were purchased from Suzhou SJ Biomaterials Co., Ltd (Suzhou, China). Oligo(ethylene glycol) methacrylate (OEGMA), 2-hydroxyethyl methacrylate (HEMA), Anhydrous N, N'-dimethylformamide (DMF), 4-(dimethylamino)pyridine (DMAP) were purchased from Aldrich. Bovine serum albumin (BSA), Rabbit anti-BSA, Streptavidin (SA), biotin, biotin-labeled Goat anti-Rabbit IgG and Rabbit IgG were purchased from Bioss (Beijing, China). N-ethyl-N'-[3-(dimethylamino)-propyl]-carbodiimide (EDC) and hydroxy-2,5-dioxopyrolidine-3-sulfonicacid sodium salt (NHSS) were purchased from Medpep (Shanghai, China). Glycine (Gly) was purchased from Dingguo (Beijing, China).

Surface preparation

The PEG-based matrix was prepared as we previously described [20], and a brief overview of the preparation of the QCM and SPR chips is provided here. The Au-coated QCM or SPR chips were immersed into a 1 mM mixed solution of initiators ω-mercaptoundecyl bromoisobutyrate and EG3-thiol to form an initiator SAM. We utilized binary mixed SAMs to systematically vary the surface density of initiators to control the density of polymer chains. In this study, we defined a solution ratio of initiator χ_I^{Sol} =0.5% and 5% (where $\chi_I^{Sol} = n_I/(n_I + n_{EG3})\times 100\%$) to represent the low density and high density matrix respectively. Surface initiated polymerization from SAM was conducted under follow procedure: To a Schlenk tube containing Milli-Q-water (5 mL), methanol (5 mL) were added, bipyridine (~12.5 mg, 0.8 mmol), and monomers OEGMA526 (2.65 g, 5 mM) and HEMA (0.65 g, 5 mM).We added a further 1 mL of $CuCl_2$ (0.04 mM) to the mixed solution. The resulting mixed solution was bubbled with nitrogen for 15 min. 1 mL of ascorbic acid (AscA; 0.04 mM) was injected with a syringe. This mixture was then transferred to a reaction setup in an inert gas glove box, and SIP was initiated and continued for a specified time at room temperature. The matrix was characterized with AFM and ellipsometer (data not shown). The thickness of the resulting matrix were 10 nm and 17 nm for low and high density, respectively. To prepare biotin surface, the resulting PEG-based matrix was prepared by immersing it in dry DMF solution containing 0.1 M biotin, 0.1 M EDC and 0.1 M DMAP for 12 h at room temperature. To prepare carboxyl-functional surface, the PEG-based matrix was incubated into a DMF solution containing succinic anhydride (10 mg mL^{-1}) and DMAP (15 mg mL^{-1}) for 12 h.

QCM Study

The biotin functionalized QCM chip was placed in a Q-Sense E4 sensor (Q-Sense, Gothenburg, Sweden) and the temperature was set to 25 °C. The QCM was operated in a flow-through mode. A baseline was established by passing PBS buffer (pH = 7.4) at a speed of 40 μL min^{-1}. SA was then injected via a Rheodyne 7125 injection valve, and the series concentrations of SA were as follows: 100 μg mL^{-1}, 50 μg mL^{-1}, 20 μg mL^{-1} and 10 μg mL^{-1}. PBS buffer was finally passed through to establish the second stable baseline.

SPR Study

SPR measurements were performed with a BIAcore 3000 to investigate the efficiency of regeneration and study the interactions between the Goat anti-Rabbit IgG and Rabbit IgG. The COOH functionalized SPR chip was placed in a BIAcore 3000 and the temperature was set to 25 °C. The running buffer was PBS (pH = 7.4) at a flow rate of 10 μL min^{-1}. The carboxyl groups were activated by a 5 min injection of an aqueous mixture of EDC (0.1 M) and NHSS (0.2 M). Then, IgG (20 μg mL^{-1}) was introduced over the activated surface, followed by ethanol amine (EtAmine at 1M, pH = 8.5) to deactivate any remaining active carboxyl groups. Anti-IgG was then introduced. In order to reuse the sensor chip, the sensor surface was then regenerated by washing with Gly (100 mM, pH = 2.0) to remove bound anti-IgG.

Results and Discussion

To test the impact of the viscoelasticity change, we first tested two types of biotin functionalized QCM chips, which were of different PEG coating density and biotin density (Scheme 1). The strong affinity binding between biotin and SA was utilized as a model system for this study. Figure 1 indicated the frequency and dissipation responses upon the injection of SA to the biotin functionalized chips.

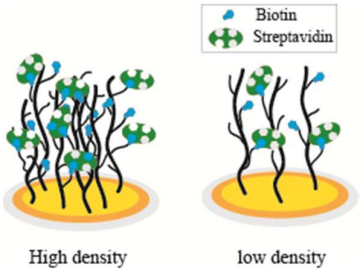

Scheme 1. The influence of the density of the matrix on QCM responses (frequency and dissipation changes) upon SA binding. In both types of chips, SA acted as the cross linker that increased the rigidity of the matrix after binding, which was indicated by positive B values.

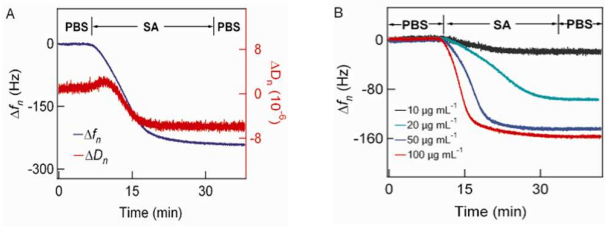

Figure 1. The values of Δf_n and ΔD_n were plotted against time (n = 3) for SA immobilization to biotin functionalized matrix. (A) a representative case of SA (100 μg mL^{-1}) binding to high density biotin chip. The blue curve is the frequency change against time and the red curve is the dissipation change against time, (B) frequency changes are responsive to SA concentration changes.

The frequency changes were then analyzed according to the impedance method (i.e., equations (1) and (2)), results shown in Figure 2. The fitted values of A and B were listed in Table 1. The value A was further converted to area averaged mass (Δm_1) according to equation (4), which was compared with the value calculated according to the Sauerbrey equation (5) (Δm_2).

$$\Delta m_1 = \rho_f d_f = \frac{Z_q A}{2 f_0^2} \qquad (4)$$

$$\Delta m_2 = C \frac{-\Delta f}{n} \qquad (5)$$

where C is a constant that depends on the thickness of the quartz and on the hydrodynamics of employed flow cells [21]. For an AT-cut 5 MHz crystal used in Q-sense flow cell, C equals is 17.7 ng cm^{-2} Hz^{-1} [22].

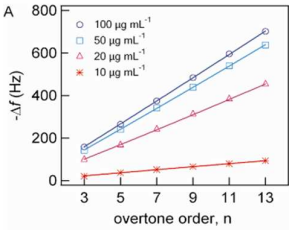

Figure 2. The values of Δf were plotted against overtone order for SA immobilized to two biotin functionalized matrices of different density. (A) low density matrix, (B) high density matrix. The frequency responses were fitted according to equation (1) for overtone numbers n = 3, 5, 7, 9, 11 and 13, (R^2 ~ 0.99). See Table 1 for fitted values of A and B.

Table 1. List of fitted values of A and B, and calculated area averaged mass increase upon SA binding to Biotin.

[SA][a]	Low Density					High Density				
	A[b]	B[b]	Δm^c	Δf^d	$\Delta m_2{}^e$	A[b]	B[b]	$\Delta m_1{}^c$	Δf^d	$\Delta m_2{}^e$
	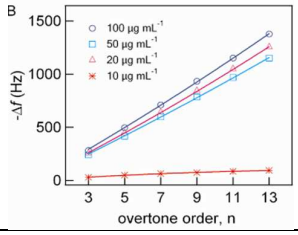									
100	52.8	0.1	950	54	964	95.3	0.8	1715	101	1827
50	47.8	0.1	860	48	874	84.6	0.9	1523	85	1539
20	33.2	0.1	598	34	615	80.9	0.6	1456	92	1650
10	7.5	0	135	7	130	11.2	-0.3	202	9	157

[a] unit is μg mL^{-1}, [b] unit is Hz, [c] the area averaged mass calculated according to equation (4). The unit is ng cm^{-2}, [d] average of 6 overtone numbers, $\Delta f = \Delta f_n/n$, n = 3, 5, 7, 9, 11 and 13. The unit is Hz, SE < 0.3, [e] the area averaged mass calculated in accordance with equation (5). The unit is ng cm^{-2}, SE < 30.Three conclusions were drawn from the above studies: First, for the tested biotin functionalized PEG matrix, viscoelasticity change induced Δf only had a minor contribution to the overall frequency change. Since fitted B values were mostly ~ 0.1 for the low density biotin chips, the contribution was less than 1 Hz for n = 3. At higher overtone numbers, such as n = 13, the contribution became ~ 17 Hz for B = 0.1. This 17 Hz change was still small compared with the overall 702 Hz change (~2%, for the low density biotin chip probed with [SA] at 100 μg mL^{-1}). No effort was made to quantitatively connect B and ΔD yet we did notice that the values of ΔD for the 8 experiments were small (0 ~ 10 × 10^{-6}, Table S1) indicating small viscoelasticity changes.

QCM was sensitive to changes of affinity binding behaviors, which caused small structural differences. Since one SA could bind up to 4 biotin molecules, we believed that partial SA acted as cross linkers because the fitted B values were mostly positive:

at high [SA] of over 20μg mL^{-1}, B values were ~ 0.1 for the low density chips and 0.6 ~ 0.9 for high density chips (Table 1). However, in the case of [SA] less than 10 μg mL^{-1}, the B value decreased to zero or negative values, indicating the binding of SA at low concentration may cause the increase in viscoelasticity of surface matrix. The A values were sensitive to the variation of [SA] for both types of chips (see supplemental information, Figure S1). Furthermore, the binding of SA to biotin caused more rigidity change for the high density matrix than the low density (i.e., ~0.7 vs. ~0.1 for B values), indicating the high density chip had a higher probability for SA to act as a cross-linker.

Although the values of area-averaged mass were close either according to equation (4) or equation (5) (less than 10% for all 8 cases in Table 1), equation (1) was still the most useful one, because it was able to correct the false signal caused by viscoelasticity change. For the case of high density biotin matrix probed with [SA] at 20 and 50 μg mL^{-1}, equation (5) gave a higher mass increase for low [SA]: 1650 ng cm^{-2} for [SA] at 20 μg mL^{-1} vs. 1539 ng cm^{-2} for [SA] at 50 μg mL^{-1}, respectively. It should be noted that the mass increase values calculated by equation (5) includes the viscoelastic contribution. After removal the viscoelastic contribution by equation (1), one can find that the surface matrix was more rigid for [SA] at 50 μg mL^{-1} (B = 0.9) than that for [SA] at 20 μg mL^{-1} (B = 0.6). Moreover, the area-averaged mass changes from A are more physically realistic by equation (4): 1456 ng cm^{-2} for [SA] at 20 μg mL^{-1} vs. 1523 ng cm^{-2} for [SA] at 50 μg mL^{-1}, respectively (Table 1).

In summarize, one could apply equation (1) to remove viscoelasticity induced contributions to frequency changes. More importantly, equation (1) only required the experiments to be carried out in multiple vibration frequencies (i.e., multiple overtone numbers), not necessary using impedance or impulse excitation techniques. Experiments were conducted to demonstrate that the biotin functionalized matrix could detect multiple step recognitions: Biotinylated anti-IgG (20 μg mL^{-1}) was applied to the SA captured biotin matrix followed by PBS for a baseline, then IgG (20 μg mL^{-1}) was passed through. We observed further frequency decrease due to the recognition between IgG and biotinylated anti-IgG. (Figure 3 and Table 2).

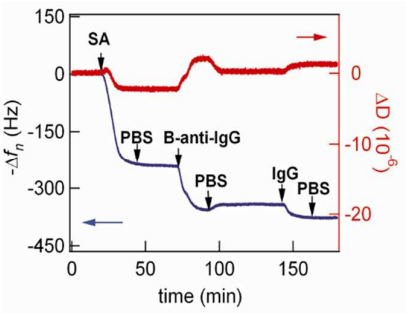

Figure 3. Demonstration of multi-step binding detections (n = 3). Biotinylated anti-IgG (20 μg mL^{-1}) were introduced to the SA captured biotin matrix, followed by PBS buffer for baseline and subsequently IgG (20 μg mL^{-1}) for the third binding. A decrease of 112 Hz and 41 Hz was recorded due to the recognition of SA /biotinylated anti-IgG pair and IgG/biotinylated anti-IgG pair, respectively.

From Table 2, the B values were all negative except a zero value, indicating that the binding of biotinylated anti-IgG caused the increase of viscoelasticity of the overall system (biotinylated PEG matrix + SA + biotinylated anti-IgG). Correspondingly, we observed all positive ΔD values (Table S1). This was reasonable because, unlike SA, biotin could not act as a cross linker. Furthermore, from Table 1, we knew that there was more SA immobilized to the high density chip. However, we found similar values of mass changes due to the binding of biotinylated anti-IgG to both high and low density chips: ~600 ng cm^{-2} and ~700 ng cm^{-2} for chips probed with 50 μg mL^{-1} and 100 μg mL^{-1} [SA], respectively (Table 2). We believed this observation was due to steric hindrance that limited the number of biotinylated anti-IgG molecules (Mw ~160 kDa) that could be packed in a relatively small space (i.e. the pseudo three dimensional polymer matrix). Similar trend was also found for the binding of IgG to immobilized biotinylated anti-IgG. (See supplemental information, Table S2)

Table 2. List of fitted values of A and B, and calculated area averaged mass increase upon the addition of biotinylated anti-IgG at 20 μg mL^{-1} to the different SA captured biotin matrix.

[SA] [a]	Low Density					High Density				
	A [b]	B [b]	Δm_1 [c]	Δf [d]	Δm_2 [e]	A [b]	B [b]	Δm_1 [c]	Δf [d]	Δm_2 [e]
100	39.2	-0.3	706	36.5	658	38.8	-0.4	698	35.5	640
50	32.9	-0.3	592	30.3	545	34.9	-0.5	629	30.9	556
20	12.1	-0.2	218	10.6	190	27.9	-0.5	502	23.2	418
10	1.2	-0.1	22	0.8	15	0	0	0	0.2	4.3

[a] unit is μg mL^{-1}, [b] unit is Hz, [c] the area averaged mass calculated according to equation (4). The unit is ng cm^{-2}, [d] average of 6 overtone numbers, $\Delta f = \Delta f_n/n$, n = 3, 5, 7, 9, 11 and 13. The unit is Hz, SE < 0.3, [e] the area averaged mass calculated in accordance with equation (5). The unit is ng cm^{-2}, SE < 30.

RSC Advances

ARTICLE

Affinity and Kinetic Rate Constants

Knoll et al. found good agreement in the affinity rate constants of perfluoropolyether lubricant Fomblin ZDOL adsorption onto a silver surface obtained by QCM and SPR. [23] Here we compared the affinity and kinetic rate constants for IgG/anti-IgG pair from QCM and SPR. The commercially available QCM and SPR chips were both functionalized with identical PEG matrices, whose preparation has been reported.[20, 24-26]

We first examined the nonfouling property of the chips (i.e., the ability to reduce/prevent nonspecific protein adsorption) and found that the PEG matrix could reduce the nonspecific protein adsorption to the level below the detection limit of QCM and SPR (Figure S2 ~ S3). Second, we optimized conditions for the immobilization of bait molecules, the binding of prey molecules as well as the regeneration of sensor chips (Figure S4 ~ S5). The optimized condition was described in details in the experimental section. Finally, we carried out a systematic study, using IgG and anti-IgG as the model bait-prey pair.

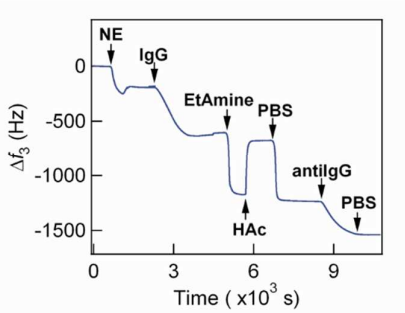

Figure 4. A typical run of bait-prey recognition study on QCM. For a COOH functionalized QCM chip, it was first probed with HAc (2 mM, pH = 4.6) as the running buffer, followed by NHSS/EDC (NE) activation. Then, IgG (50 μg mL^{-1}) was introduced, resulting in a 289.5 Hz frequency decrease. Ethanol amine (EtAmine at 1 M, pH = 8.5) was applied to deactivate remaining active carboxyl groups. The running buffer was then switched to PBS (pH = 7.4), followed by flowing through anti-IgG (50 μg mL^{-1}). After switching back to PBS, there was a 254.8 Hz frequency decrease due to bait-prey recognition.

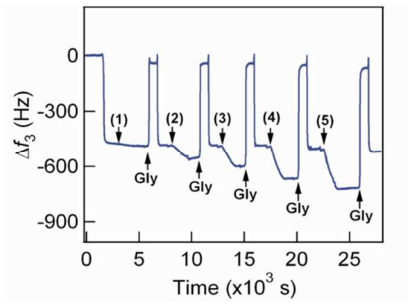

Figure 5. A typical run for affinity and kinetic rate constants determination on QCM. The procedure for bait immobilization (IgG at 50 μg mL^{-1}) was the same as Figure 4. Anti-IgG at a series of concentrations ((1) 1.0 μg mL^{-1}; (2) 6.3 μg mL^{-1}; (3) 12.5 μg mL^{-1}; (4) 25.0 μg mL^{-1}; (5) 50.0 μg mL^{-1}), Gly (100 mM, pH = 2.0) and PBS were introduced in turns. The binding curves were fitted for affinity and kinetic rate constants. (see Figure 6).

It was assumed that the frequency change has a linear relation to the amount of captured prey molecules. Liu et al.[27] applied QCM to study the kinetics of binding. Here we applied similar equations to obtain affinity and kinetic rate constants (see supplemental information for detailed equation deduction).

$$\Delta f = \frac{k_a C \Delta f_{\max}}{(k_a C + k_d)}(1 - e^{-(k_a C + k_d)\times t}) \quad (6)$$

$$Z = k_a \times C + k_d \quad (7)$$

where k_a is the association rate constant and k_d is the dissociation rate constant, C is the concentration of free prey molecules.

Earlier data analysis confirmed that the PEG matrix tested here had negligible viscoelasticity induced frequency changes. Here we found that a kinetic simulation based on fitted A values gave similar results with a kinetic simulation directly from Δf (see Figure S6). The latter is much more convenient and will be applied thereafter. We also confirmed the affinity and kinetic rate constants were independent on the overtone numbers (Table S5). Therefore, n = 3 would be used as a representative case.

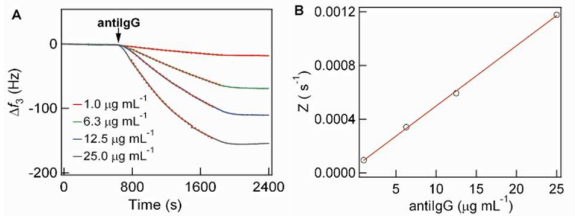

Figure 6. Curve fitting for affinity and kinetic constants determination. (A) the binding curves from Figure 5 were reconstructed for clarity and fitted according equations (6); (B) the fitted values of Z were linearly fitted, resulting in k_a, k_d and K_A ($K_A = k_a/k_d$), see Table 3 for numbers

Table 3. Affinity and kinetic rate constants of the binding between IgG and anti-IgG

IgG (μg mL^{-1})	25	50	125	250
Δf_3 (Hz)[a]	253.5	289.5	458.9	507.1
k_a (μg^{-1} mL s^{-1}	4.0×10^{-5}	4.6×10^{-5}	3.0×10^{-5}	3.0×10^{-5}
k_d (s^{-1})	5.0×10^{-5}	7.4×10^{-5}	1.0×10^{-4}	2.0×10^{-4}
K_A (M^{-1})	1.2×10^{8}	9.3×10^{7}	4.5×10^{7}	2.3×10^{7}
R^2	0.996	0.982	0.979	0.941

[a] frequency response upon IgG immobilization.

The potential impact of the immobilized density of bait molecules was tested by varying the concentration of bait molecules at the immobilization step. For example, we tested IgG immobilization at 25, 50, 125, 250 μg mL^{-1}, resulting in different densities of immobilized IgG as evident from the different value of Δf_3 (Table 3). These surfaces were then probed with the same concentration series of prey molecules. It gave similar association rate constants and was in agreement with reported findings that when the prey molecule concentration was too high , affinity constants could be relatively small. The dissociation rate constant, however, varied according to the density of immobilized IgG: a 4 fold increase when the IgG concentration increased from 25 to 250 μg mL^{-1}. Steric effect may be one of the causes for the observed concentration dependence, which should be more pronounces at high matrix concentration as it more greatly affects the penetration of the analyte protein. The same bait-prey pair was tested in a BIAcore 3000 SPR. The kinetic rate constants calculated from QCM and SPR were slightly different: SPR gave a 10 fold larger k_a value and 30 fold larger k_d value than QCM results. This may be explained by employment of different flow cells in QCM and SPR. As we known, BIAcore 3000 using microfluidic channel with a high flow rate. High flow rate has dual functionality: (1) to drive analyte to the chip surface, and to let them interact with immobilized antibodies, and (2) to force the dissociation of formed bonds and to detach bound analyte from surface. As a result, both association and dissociation obtained by SPR are higher than those in QCM. However, the equilibrium constant K_A was similar, because the flow effect is canceled by taking a ratio between k_a and k_d. The results indicated that the affinity values using QCM and SPR are valid.

We further studied the potential impact of immobilization on bait-prey recognition. First, anti-IgG was immobilized as the bait molecules and tested with IgG as the prey molecule. It gave similar affinity rate constants, but kinetic rate constants were slightly different (Table S6). This discrepancy was attributed to the difference of molecular in weight, shape and size, which resulted in different steric hindrance after the immobilization. Generally speaking, when proteins with small molecular weights were used as prey, they were able to diffuse into matrix easier, and interact with the baits.[28] In another test, anti-BSA was able to bind to BSA, which was immobilized to surface as bait molecule. However, BSA was unable to bind to anti-BSA when anti-BSA was used as bait molecule (Figure S8). Thus, when using surface-sensitive method to detect the affinity constants, choice suitable ligand should be taken into account when designing experiment.

Conclusions

In conclusion, it is demonstrated that the impedance analysis of frequency changes at multiple overtone numbers was practicable for biomolecular interaction study. This method could be applied to separate the frequency change due to mass deposition and viscoelasticity changes. While impedance analysis (or D factor) was required to monitor viscoelasticity change, frequency changes at multiple overtone numbers were sufficient to indicate if there were significant viscoelastic contributions. The experimental data consistently indicated these factors could be minimized for a properly designed matrix. Furthermore, the presented equation is advantageous in that it can analyse single data point while the Voigt model method requires at least three points of different film thickness, which was a formidable challenge for most biological samples.[29, 30] Using model bait-prey pairs, we demonstrated the potential value of QCM as a biosensor for quantitative analysis of biomolecular interactions. Due to its affordability and the opportunity for accurate analysis with the PEG matrix, we believed that the PEG matrix and the equations (for impedance analysis of frequency changes at multiple overtones) will facilitate the popularization of QCM as a biosensor in biomolecular interaction study for its affordability.

Acknowledgements

We thank Y.Z. Zhang for his help in valuable feedback in this study. This work was supported by Shenzhen science and technology Foundation (No. JCYJ20140419151618022), the National Natural Science Foundation of China (No. 21444007), the Natural Science Foundation of Jiangsu Province (No. BK20130345), Shenzhen science and technology R&D Foundation (No. ZYA201106080020A) and Project supported by Shenzhen enter-exit inspection and quarantine bureau (No.SZ2014101)

1. J. Homola, S. S. Yee and G. Gauglitz, *Sensors and Actuators B-Chemical*, 1999, **54**, 3-15.
2. E. Reimhult, C. Larsson, B. Kasemo and F. Hook, *Anal. Chem.*, 2004, **76**, 7211-7220.
3. L. M. Pandey and S. K. Pattanayek, *Journal of Chemical & Engineering Data*, 2013, **58**, 3440-3446.
4. J. He, Y. Lu, J. Fang and H. Ma, *Science China-Chemistry*, 2012, **55**, 175-181.
5. J. Fang, C. Ren, T. Zhu, K. Wang, Z. Jiang and Y. Ma, *Analyst*, 2015, **140**, 1323-1336.
6. Y. Luan, D. Li, Y. Wang, X. Liu, J. L. Brash and H. Chen, *Langmuir : the ACS journal of surfaces and colloids*, 2014, **30**, 1029-1035.
7. H. Szalontai, N. Adányi and A. Kiss, *New Biotechnology*, 2014, **31**, 395-401.
8. F. Hook, B. Kasemo, T. Nylander, C. Fant, K. Sott and H. Elwing, *Anal. Chem.*, 2001, **73**, 5796-5804.
9. G. Duner, E. Thormann and A. Dedinaite, *Journal of colloid and interface science*, 2013, **408**, 229-234.
10. Y. K. Suh, B. C. Kim and Y. H. Kim, *Sensors*, 2009, **9**, 9544-9558.
11. F. Caruso, E. Rodda, D. N. Furlong and V. Haring, *Sensors and Actuators B (Chemical)*, 1997, **B41**, 189-197.

12. L. E. Bailey, D. Kambhampati, K. K. Kanazawa, W. Knoll and C. W. Frank, *Langmuir : the ACS journal of surfaces and colloids*, 2002, **18**, 479-489.
13. M. Muratsugu, F. Ohta, Y. Miya, T. Hosokawa, S. Kurosawa, N. Kamo and H. Ikeda, *Analytical chemistry*, 1993, **65**, 2933-2937.
14. N. C. Fawcett, R. D. Craven, P. Zhang and J. A. Evans, *Analytical chemistry*, 1998, **70**, 2876-2880.
15. M. J. Shuster, A. Vaish, M. E. Szapacs, M. E. Anderson, P. S. Weiss and A. M. Andrews, *Advanced Materials*, 2008, **20**, 164-167.
16. B. S. Lee, Y. S. Chi, K. B. Lee, Y. G. Kim and I. S. Choi, *Biomacromolecules*, 2007, **8**, 3922-3929.
17. M. Tabrizian, S. D. Carrigan and G. Scott, *Biomaterials*, 2005, **26**, 7514-7523.
18. M. Suhr, N. Unger, K. E. Viacava, T. J. Gunther, J. Raff and K. Pollmann, *Biometals*, 2014, **27**, 1337-1349.
19. Y. Zhang, B. Du, X. Chen and H. Ma, *Anal. Chem.*, 2009, **81**, 642-648.
20. H. Ma, J. a. He, X. Liu, J. Gan, G. Jin and J. Zhou, *ACS Appl. Mat. Interfaces*, 2010, **2**, 3223-3230.
21. C. Malitesta, R. A. Picca, E. Mazzotta and M. R. Guascito, *Electroanalysis*, 2012, **24**, 790-797.
22. G. Zelander, Nat. Methods, 2006, 41-42.
23. X. D. Su, Y. J. Wu and W. Knoll, *Biosensors & Bioelectronics*, 2005, **21**, 719-726.
24. X. Liu, T. Li, D. Liu and Z. Wang, *Anal. Methods*, 2013, **5**, 285-290.
25. A. Larsson, C.-X. Du and B. Liedberg, *Biomacromolecules*, 2007, **8**, 3511-3518.
26. H. W. Ma, J. H. Hyun, P. Stiller and A. Chilkoti, *Adv. Mater.*, 2004, **16**, 338-341.
27. Y. Liu, X. Yu, R. Zhao, D. H. Shangguan, Z. Y. Bo and G. Q. Liu, *Biosensors & Bioelectronics*, 2003, **19**, 9-19.
28. A. W. Drake, M. L. Tang, G. A. Papalia, G. Landes, M. Haak-Frendscho and S. L. Klakamp, *Anal. Biochem.*, 2012, **429**, 58-69.
29. Z. Cao, T. Tsoufis, T. Svaldo-Lanero, A.-S. Duwez, P. Rudolf and K. Loos, *Biomacromolecules*, 2013, **14**, 3713-3722.
30. L.-J. Gu, J. Wang and H.-W. Ma, *Chin. J. Anal. Chem.*, 2013, **41**, 956-962.